

# ExoMol line lists XXIV: A new hot line list for silicon monohydride, SiH

Sergei N. Yurchenko<sup>1</sup>, Frances Sinden<sup>1</sup>, Lorenzo Lodi<sup>1</sup>, Christian Hill<sup>1</sup>, Maire N. Gorman<sup>2</sup>, and Jonathan Tennyson<sup>1</sup>

<sup>1</sup> *Department of Physics and Astronomy, University College London, Gower Street, London, UK, WC1E 6BT*

<sup>2</sup> *Department of Physics, Aberystwyth University, Penglais, Aberystwyth, Ceredigion, UK, SY23 3BZ*

Accepted XXXX. Received XXXX; in original form XXXX

## ABSTRACT

SiH has long been observed in the spectrum of our Sun and other cool stars. Computed line lists for the main isotopologues of silicon monohydride, <sup>28</sup>SiH, <sup>29</sup>SiH, <sup>30</sup>SiH and <sup>28</sup>SiD are presented. These line lists consider rotation-vibration transitions within the ground  $X^2\Pi$  electronic state as well as transitions to the low-lying  $A^2\Delta$  and  $a^4\Sigma^-$  states. *Ab initio* potential energy (PECs) and dipole moment curves (DMCs) along with spin-orbit and electronic-angular-momentum couplings between them are calculated using the MRCI level of theory with the MOLPRO package. The PEC for the ground  $X^2\Pi$  state is refined to available experimental data with a typical accuracy of around 0.01 cm<sup>-1</sup> or better. The <sup>28</sup>SiH line list includes 11,785 rovibronic states and 1,724,841 transitions with associated Einstein-A coefficients for angular momentum  $J$  up to 82.5 and covering wavenumbers up to 31340 cm<sup>-1</sup> ( $\lambda < 0.319 \mu\text{m}$ ). Spectra are simulated using the new line list and comparisons made with various experimental spectra. These line lists are applicable up to temperatures of 5000 K, making them relevant to astrophysical objects such as exoplanetary atmospheres and cool stars and opening up the possibility of detection in the interstellar medium. These line lists are available at the ExoMol ([www.exomol.com](http://www.exomol.com)) and CDS database websites.

**Key words:** molecular data; opacity; astronomical data bases: miscellaneous; planets and satellites: atmospheres; stars: low-mass

## 1 INTRODUCTION

Silicon hydride (SiH) is a free radical formed from the cosmically abundant elements of hydrogen and silicon, and is the simplest of the four possible silicon hydrides. Following the first experimental measurement of the  $A^2\Delta - X^2\Pi$  system of SiH by Jackson (1930), SiH was observed by Pearse (1933) and Babcock (1945) in sunspots and in the spectrum of the solar disk spectrum by Schadee (1964) and Moore-Sitterly (1966). These identifications were then corroborated by Sauval (1969) using the coincidence method and also by Lambert & Mallia (1970), who derived oscillator strengths and isotope shifts for <sup>29</sup>SiH and <sup>30</sup>SiH. Furthermore, Grevesse & Sauval (1970) observed SiH in the photospheric region of the sun and also subsequently calculated oscillator strengths (Grevesse & Sauval 1971).

SiH has been observed in late-type stars by Davis (1940) and in the emission spectra of M- and S-type Mira variable stars (Merrill 1955). SiH is also important for the modelling of M-dwarf atmospheres (Allard & Hauschildt 1995), although of less importance than species with more pronounced spectroscopic features. In exoplanetary and brown dwarf atmospheres Visscher et al. (2010) make the prediction that SiO should be the most abundant silicon species in low pressure environments, with silane (SiH<sub>4</sub>) the most abundant at high pressures. They also predict that SiH may be present due to equilibrium reactions of SiH with both SiH<sub>4</sub> and SiO in the presence of H<sub>2</sub>O.

In the interstellar medium (ISM), given the observations of similar molecules such as SiO, CH and OH, the presence of SiH has been suggested by numerous authors (Wilson et al. 1971; Weinreb et al. 1963; Rydbeck et al. 1973; Lovas 1974; Turner & Dalgarno 1977; de Almeida & Singh 1978). In particular, Herbst et al. (1989) suggested that the abundances of both silicon and hydrogen make SiH a likely candidate to be found in interstellar clouds, where it so far remains undetected.

Several theoretical studies exploring the electronic and thermodynamic properties of SiH have been made, often as parts of larger studies of silicon hydrides. The first *ab initio* electronic structure calculations were performed by Cade & Huo

(1967) who produced a ground state potential energy curve (PEC) using the Hartree-Fock method and Slater-type orbital basis functions. Ramakrishna Rao & Lakshman (1971) used the Rydberg-Klein-Rees method as well as their own modified method to calculate the PECs for the  $X^2\Pi$  and  $A^2\Delta$  states for SiH on the basis of the known experimental data. Later Meyer & Rosmus (1975) used the coupled electron pair approximation (CEPA) method and a Gaussian-type orbital (GTO) basis set to examine both the PEC and DMC of the SiH ground state. This work on the PEC for the ground state has been followed up by Shi et al. (2008) and Prascher et al. (2009) using the coupled-cluster method, with the latter of these studies forming part of a more general, larger study of silicon-containing hydrides. Additionally, theoretical calculations of the ground state dipole were also performed by several authors using various methods (Meyer & Rosmus 1975; Kalcher 1987; Ajitha & Pal 1999; Park & Sun 1992; Pettersson & Langhoff 1986). The transition dipole between the  $X^2\Pi$  and  $A^2\Delta$  states for SiH was calculated by Larsson (1987) using the CASSCF method. Buenker (1986) used SiH as a test case for his theoretical study on the calculation of excited molecular states.

A considerable step forward was made by Kalemos et al. (2002), who used the multi-reference configuration interaction (MRCI) method to compute 16 electronic states of SiH. More recently, Shi et al. (2013) produced PECs for seven bound states of SiH and gave a new set of spectroscopic parameters using, again, the MRCI method (aug-cc-pV6Z basis set for Si and aug-cc-pV5Z for H) and accounting for spin-orbit coupling using the Breit-Pauli Hamiltonian.

Spin-orbit coupling in SiH has also been specifically studied by several authors (Chang & Sun 2003; Song et al. 2008; Stevens & Krauss 1982; Shi et al. 2013); more general studies of spin-orbit coupling in diatomic molecules have been undertaken by Brown & Watson (1977), Qui-Xia et al. (2008), Baek & Lee (1990) and Chang & Sun (2008). A splitting in SiH was calculated by Wilson & Richards (1975), complementing various experimental measurements (Freedman & Irwin 1976; Klynning et al. 1979; Cooper & Richards 1981).

SiH is of considerable interest to the semiconductor industry and it is a by-product in the production of thin films for devices such as LCDs (Jasinski et al. 1995; Turban et al. 1980, 1981; Drevillon & Toulemonde 1985). Neutral radicals, particularly SiH<sub>3</sub> provide the most efficient growth in the chemical vapour deposition process, with SiH only occurring in comparatively negligible quantities (Robertson & Gallagher 1986). It is usually produced from SiH<sub>4</sub> using photolysis, radio frequency discharge, or by equilibrium reaction with fluorine (Kalemos et al. 2002). Numerous studies of SiH within silane plasmas has been undertaken (Taniguchi et al. 1980; Matsuda et al. 1980; Kampas & Griffith 1981; Schmitt et al. 1984) and also of thermodynamic properties such as bond strength, enthalpies and heats of formation of silicon-containing hydrides (Husain & Norris 1979; McMillen & Golden 1982; Sax & Kalcher 1991; Leroy et al. 1992; Grant & Dixon 2009; Jun et al. 2010).

Experimentally, rovibrational transition wavelengths for SiH within the ground state were measured extensively during the 1980s (Brown & Robinson 1984; Brown et al. 1984; Brown et al. 1985; Davies et al. 1985; Betrencourt et al. 1986; Seebass et al. 1987). However, the first recorded wavelengths for SiH were actually for the  $A^2\Delta - X^2\Pi$  system starting with Jackson (1930), with the most recent study by Ram et al. (1998) building on earlier work (Rochester 1936; Douglas 1957; Verma 1965; Singh & Vanlandingham 1978; Klynning et al. 1979). Spectra for this system were also recorded in the gas phase as part of silane glow discharge studies (Nemoto et al. 1989; Washida et al. 1985; Perrin & Delafosse 1980; Stamou et al. 1997). Additionally, the overall absorption cross sections and electronic transition moment for this system were determined by Park (1979) using a shock tube.

Limited experimental work has been undertaken for other excited states; Bollmark et al. (1971) recorded spectra around 3250 Å which they attributed to transitions involving the  $B^2\Sigma^-$  and  $C^2\Sigma^+$  states. The  $E^2\Sigma^+ - X^2\Pi$  and  $D^2\Delta - X^2\Pi$  systems for SiH and SiD around 1907 Å and 2058 Å respectively were recorded by Herzberg et al. (1969), following earlier, preliminary work by Verma (1965). Finally, Johnson & Hudgens (1989) located a state at  $46700 \pm 10 \text{ cm}^{-1}$  which they classified as either  $^2\Pi$  or  $^2\Sigma^+$  using resonance-enhanced multiphoton ionization (REMPI) spectroscopy.

The Cologne Database for Molecular Spectroscopy (CDMS) lists 125 purely rotational transition lines within the vibrational ground state spanning the 0.2–5275 GHz range (radio and microwave spectral range) (Müller et al. 2005). Kurucz (2011) has compiled a larger line list of 78,286 transitions, last updated in 1998 for  $J$  up to 37.5. Oscillator strengths and Franck-Condon factors have been measured by Smith & Liszt (1971) whilst measurements of lifetimes have been recorded by Smith (1969) and Bauer et al. (1984), Nemoto et al. (1989).

The ExoMol project aims at providing line lists of spectroscopic transitions for key molecular species which are likely to be important in the atmospheres of extrasolar planets and cool stars (Tennyson & Yurchenko 2012; Tennyson et al. 2016c). This is essential for the continued exploration of newly discovered astrophysical objects such as exoplanets, for which there is an increasing desire to characterise their atmospheric compositions. The methodology of the line list production for diatomics is discussed by Tennyson & Yurchenko (2017). ExoMol has already provided rotation-vibration line lists for the closed shell silicon-containing molecules SiO (Barton et al. 2013) and SiH<sub>4</sub> (Owens et al. 2017). Given the astronomical interest in SiH, we present a new line list for SiH applicable for temperatures up to 5000 K.

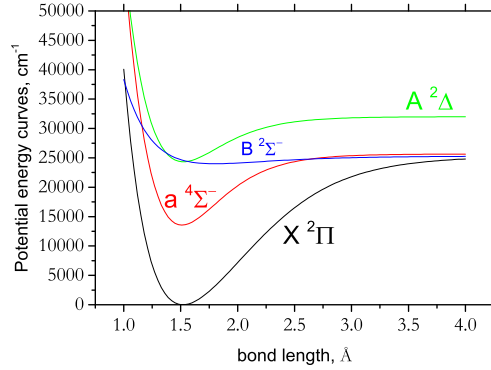


**Figure 1.** Potential energy curves of SiH used in the line list production. The  $X^2\Pi$  and  $A^2\Delta$  PECs have been refined, the  $a^4\Sigma^-$  is *ab initio* and the  $B^2\Sigma^-$  PEC is an artificial object used to improve the description of the  $\Lambda$ -doubling in the  $X$ -state spectra (see section 4).

## 2 METHOD

The procedure used here for the calculation of SiH line lists is the established ExoMol methodology of refining *ab initio* results to available experimental data. Because of the absence of a complete set of potential energy curves (PECs), dipole moment curves (DMCs), spin-orbit curves (SOC) and electronic angular momentum coupling curves (EAMC) in the literature, *ab initio* calculations of the four lowest-lying electronic states were performed using the program MOLPRO (Werner et al. 2010, 2012).

The *ab initio* PEC, SOC, and EAMC curves were produced at the MRCI level of theory in conjunction with the aug-cc-pwCVQZ basis sets (Dunning 1989; Woon & Dunning 1993; Peterson & Dunning 2002) with relativistic, core-correlation effects and Davidson correction taken into account. The PECs of  $X^2\Pi$  and  $A^2\Delta$  as well as SOC, EAMCs between the  $X$ ,  $A$ , and  $B$  states were then refined using DUO (Yurchenko et al. 2016) and the available experimental data.

## 3 DIPOLE MOMENT CURVES

The DMC of the  $X^2\Pi$  state was computed using MRCI/aug-cc-pwCV5Z-DK (Dunning 1989; Raghavachari et al. 1989) with the core-correlation and relativistic effects, the latter using the Douglas-Kroll-Hess method (Reiher 2006) and including the Davidson correction (Langhoff & Davidson 1974). The finite field method was used. For a discussion of the calculation of DMCs using the expectation and finite field methods see Lodi & Tennyson (2010).

The dipole moment for the  $X^2\Pi$  state and the transition dipole moment between the  $A^2\Delta - X^2\Pi$  state are shown in Fig. 2. Our equilibrium value of the  $X^2\Pi$  DMC is 0.097 D. Previous theoretical estimates range between 0.076 D (Allen et al. 1986) and 0.173 D (Ajitha & Pal 1999) with other estimates being 0.122 D (Larsson 1987; Park & Sun 1992), 0.125 D (Mauricio et al. 1988), 0.117 D (Pettersson & Langhoff 1986), 0.140 D (Meyer & Rosmus 1975) and 0.160 D (Huzinaga 1965).

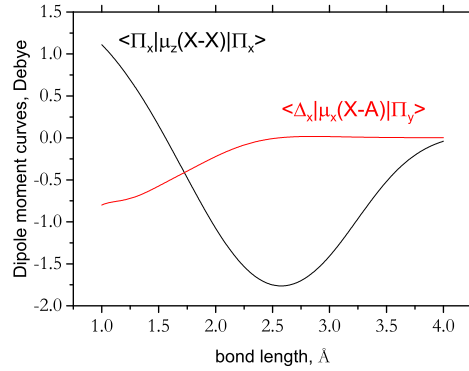
The *ab initio* transition dipole moment components  $\mu_\alpha$  between the  $A^2\Delta$  and  $X^2\Pi$  states can be defined as the matrix elements between the Cartesian  $|\Delta_\alpha\rangle$  and  $|\Pi_\alpha\rangle$  components of the corresponding electronic eigenfunctions (where  $\alpha = x, y, z$ ), which is also MOLPRO's basis set convention. For the 'equilibrium' value of  $\langle\Delta_z|\mu_y|\Pi_y\rangle$  (taken at  $r = 1.52$  Å) we obtained 0.585 D. This matrix element is connected to the spherical tensor dipole representation by

$$\langle\Lambda = 2|\mu_+|\Lambda = 1\rangle = \sqrt{2}\langle\Delta_x|\mu_y|\Pi_y\rangle = 0.827 \text{ D}, \quad (1)$$

where  $\mu_+ = (-\mu_x + i\mu_y)/\sqrt{2}$ . Here  $|1\rangle \equiv |^2\Pi\rangle$  and  $|2\rangle \equiv |^2\Delta\rangle$  are eigenfunctions of the  $\hat{L}_z$  operator and also linear combinations of  $|\Pi_x\rangle, |\Pi_y\rangle$  and  $|\Delta_z\rangle, |\Delta_{xy}\rangle$ , respectively. The tensorial representation of the dipole moment ( $\mu_+$ ) has been generally recommended (Whiting et al. 1980). Larsson (1987) obtained a CASSCF value of  $\mu_+ = 0.706$  D using a 5-electrons in 9 orbitals ( $3\sigma, 2\pi, 1\delta$ ) active space (see Table V of cited paper) and a basis set approximately equivalent in size to the cc-pVTZ one. It should be noted that the latter value better reproduces the observed  $A-X$  lifetime (see discussion below). As suggested by Larsson (1987), it is important to include at least one set of (doubly degenerate)  $\delta$  orbitals into CAS. We also found a strong variation of the  $A-X$  transition dipole with respect to the active space used. Our final choice for the active space was a rather large 5-electrons in 15 orbitals complete active space comprising ( $C_{2v}$  symmetry labels) 8  $a_1$ , 3  $b_1$ , 3  $b_2$  and 1  $a_2$  active orbitals; the five core orbitals (3 of  $a_1$  symmetry and one for both  $b_1$  and  $b_2$  symmetries) were kept doubly occupied (i.e., excluded from the active space). CASSCF calculations used state-averaging over the lowest  $\Sigma^+$ ,  $\Sigma^-$ ,  $\Pi$  and  $\Delta$  states. Our choice of active space was also motivated by reason of numerical stability and convergence of the calculations (see also the discussion at the end of section 5). The aug-pV(Q+d)Z basis set was used. Core-correlation and relativistic corrections

**Table 1.** Expansion parameters of the dipole moment functions,  $X-X$   $\langle \Pi_x | \mu_z | \Pi_x \rangle$  and  $X-A$   $\langle \Delta_x | \mu_y | \Pi_y \rangle$ , see Eq. (2). The units are Å and Debye.

Parameter	$X-X$	$X-A$
$r_{\text{ref}}$	1.5202	1.5202
$\beta_2$	0.216	0.460
$\beta_4$	0.05979580	0.01
$p$	1	8
$d_0$	0.0970036013	0.4857112345
$d_1$	-2.3766347830	0.5013535548
$d_2$	-1.3617433491	0.7190055685
$d_3$	0.1146612097	0.1181888386
$d_4$	0.1371530465	-2.2686306105
$d_5$	0.2436343227	-2.2419525352
$d_6$		2.3729868957
$d_\infty$	0	0

**Figure 2.** Dipole moment curve (DMC) calculated for the  $X$   $^2\Pi$  state and the transition dipole moment (TDM) for the  $A$   $^2\Delta - X$   $^2\Pi$  state.

had only marginal effects and were not taken into account for this property. In any case contributions from these effects tend to cancel (Tennyson 2014).

In order to reduce the numerical noise when computing the line-strengths using the DUO program, we followed the recommendation by Medvedev et al. (2016) and represented these two DMCs analytically. The following expansion with a damped-coordinate was employed to represent our dipole moment functions:

$$\mu(r) = (1 - \xi) \sum_{n \geq 0} d_n z^n + d_\infty \xi, \quad (2)$$

where  $\xi$  is the Šurkus variable (Šurkus et al. 1984)

$$\xi = \frac{r^p - r_{\text{ref}}^p}{r^p + r_{\text{ref}}^p} \quad (3)$$

with  $p$  as a parameter, and  $r_{\text{ref}}$  as a reference position and  $z$  is given by

$$z = (r - r_{\text{ref}}) e^{-\beta_2(r - r_{\text{ref}})^2 - \beta_4(r - r_{\text{ref}})^4}. \quad (4)$$

The expansion parameters  $d_n$ ,  $d_\infty$  (the value of the dipole at  $r \rightarrow \infty$ ),  $\beta_2$  and  $\beta_4$  (damping factors) are collected in Table 1 and are given in supplementary material as part of the DUO input file, while the functional form has been implemented into DUO.

The PECs shown in Fig. 1 are those calculated in this work with the  $X$   $^2\Pi$  and  $A$   $^2\Delta$  states having been refined,  $a$   $^4\Sigma^-$  is *ab initio* and  $B$   $^2\Sigma^-$  is a reference curve used to improve the description of the  $\Lambda$ -doubling (see discussion below). Qualitatively, in terms of general behaviour these compare favourably to Kalemios et al. (2002) who used larger basis sets (aug-cc-pV5Z and aug-cc-pV6Z) to calculate a number of PECs and SOCs for the low-lying electronic states of SiH.

#### 4 REFINEMENT

In order to refine our model for the  $X$   $^2\Pi$  and  $A$   $^2\Delta$  states the experimental frequencies were collected from the papers given in Table 2. These measurements span  $J$  up to 18.5 in the  $(0-1)$ ,  $(0-1)$  and  $(1-1)$  bands, and  $J$  up to 10.5 in the  $(2-0)$  and

**Table 2.** Summary of Experimental Data used for refining the *ab initio*  $X^2\Pi$  PEC of SiH. CTS=Czerny-Turner spectrograph, DLAR=diode laser absorption spectroscopy, FTS=Fourier Transform Spectrometer

Study	Method	System	J	$\nu$	Wavenumber Range ( $\text{cm}^{-1}$ )
Klynning et al. (1979)	CTS	$A^2\Delta-X^2\Pi$	0.5 – 14.5	(0,0)	23 958 – 24 399
Davies et al. (1985)	DLAR	$X^2\Pi - X^2\Pi$	0.5 – 9.5	(1, 0)	1838 – 2094
Betrencourt et al. (1986)	FTS	$X^2\Pi - X^2\Pi$	0.5 – 15.5	(1,0), (2, 1), (3, 2)	1704 – 2142
Ram et al. (1998)	FTS	$A^2\Delta-X^2\Pi$	1.5 – 18.5	(0, 0), (1, 1)	23 644 – 24 461

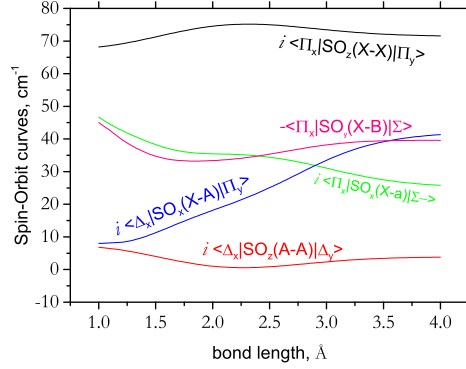


**Figure 3.** The SO couplings (Cartesian representation as computed by MOLPRO). The X-X, X-A, X-B SOC were refined.

(3 – 2) bands. Using the MARVEL program (Measured Active Rotational-Vibrational Energy Levels) (Furtenbacher et al. 2007; Furtenbacher & Császár 2012), 337 energy levels were determined from 894 transitions.

The *ab initio* PECs, SOC and EAMCs were refined by fitting to these derived MARVEL energy levels, which were then complemented with the original experimental frequencies. We used the Extended Morse Oscillator (EMO) analytical function to represent the PECs in the fits, which has the form

$$V(r) = V_e + (A_e - V_e) \left[ 1 - \exp \left( - \sum_{k=0}^N B_k \xi^k (r - r_e) \right) \right]^2, \quad (5)$$

where  $D_e = A_e - V_e$  is the dissociation energy,  $r_e$  is an equilibrium distance of the PEC, and  $\xi$  is the Šurkus variable with  $r_{\text{ref}} = r_e$ . Note that  $p$  and  $N$  can have different values in the short ( $r \leq r_e$ ) and long ( $r > r_e$ ) regions, i.e.  $p_s(N_s)$  and  $p_l(N_l)$ , respectively. The parameters are given as supplementary data together with the actual PECs for convenience.

During the fitting of the  $X$  and  $A$  states, various electronic couplings involving this electronic state were included. The refined coupling curves are shown in Figs. 3 and 4. To represent the X-X and A-A SOC, the expansion in Eq. (2) was used. The non-diagonal X-a, X-A, X-B SOC as well as the EAMCs were morphed using the following expansion in terms of the Šurkus variable:

$$F(\xi) = (1 - \xi) \sum_{k=0}^N B_k \xi^k + \xi B_\infty. \quad (6)$$

The expansion parameters are given in supplementary material as part of the DUO input file.

For  $\Pi$  states  $\Lambda$ -doubling is predominantly caused by the interaction with  $\Sigma$ -states (Brown & Merer 1979). In the case of  $X^2\Pi$  of SiH, the closest  $\Sigma$  state is  $B^2\Sigma^-$ . This interaction is still much weaker than the SO coupling, giving splittings of roughly  $0.1 \text{ cm}^{-1}$  for  $J = 0.5$  (see Table 4) with the two components having almost the same intensity (Verma 1965). Theoretically, excited states such as the  $A^2\Delta$  should also exhibit  $\Lambda$ -doubling, although because of the small splittings this has been difficult to observe experimentally.

The EAM coupling between the  $B^2\Sigma^-$  and  $X^2\Pi$  states is shown in Fig. 4. Since the  $B^2\Sigma^-$  PEC is weakly bound and DUO currently can only work with properly bound potential energy curves, we used a dummy curve with a shallow minimum for the  $B^2\Sigma^-$  PEC as a reference object. This was sufficient to produce the correct  $\Lambda$ -doubling effect for all  $J$  values considered. It should be noted that inclusion of an effective  $\Lambda$ -doubling curve is available in DUO (Yurchenko et al. 2016) but did not produce a correct  $J$ -dependence and therefore was discarded. In order to model the X-B EAM coupling the Šurkus-expansion in Eq. (6) was used.

As well as SO and EAMC, other empirical corrections such as Born-Oppenheimer breakdown (BOB) (Le Roy 2007) and spin-rotation (SR) (Kato 1993) were used to provide greater accuracy, see Yurchenko et al. (2016). The SR within the  $X$  state and the X-X and A-A SO couplings were represented by the form given by Eq. (2) with the remaining SOC, EAMC, SR



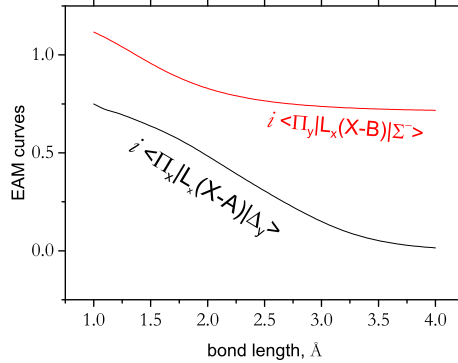


**Figure 4.** Electronic angular momentum coupling curves (EAMC) couplings (Cartesian representation as in MOLPRO). Both the  $X-A$  and  $X-B$  EAMCs were refined.

and the BOB curves were represented by Eq. (6). The parameters obtained as well as all curves specifying our final model form part of the DUO inputs are provided in the supplementary material.

The dissociation energy is poorly constrained by the low-lying vibrational state included in the fit. Initially the  $D_0$  value was set to the experimental estimate of 2.98 eV ( $\pm 0.03$  eV) from Berkowitz et al. (1987) and then allowed to float to values near this value. Our final value for the dissociation energy  $D_0$  for the  $X$  state is 3.020 eV, which corresponds to  $D_e = 3.136$  eV and the zero-point energy of  $941.23 \text{ cm}^{-1}$  ( $v = 0, J = 0.5, +$ ). Our final dissociation energy  $D_0$  of the  $A$  state is 0.84 eV ( $D_e = 0.95$  eV).

Figure 5 offers a visual comparison of the Obs.-Calc. residuals as a function of  $J$ , with the various vibrational and vibronic bands are indicated. Table 3 presents a representative sample of data for low  $J$  for  $v = 0$  showing the comparison and table 4 demonstrates the accuracy when the vibrational number  $v$  is varied. 400  $X-X$  transition wavenumbers ( $J' \leq 16.5$ ) are reproduced with the root-mean-square (rms) error of  $0.015 \text{ cm}^{-1}$ , 51 pure rotational energies ( $J \leq 11.5$ ) collected from CDMS are reproduced with an rms error of  $0.005 \text{ cm}^{-1}$ , 494 rovibronic  $A-X$  transition wavenumbers ( $J' \leq 18.5$ ) are reproduced with an rms error of  $0.016 \text{ cm}^{-1}$ . The accuracy of the pure rotational energies is comparable to that of the typical effective Hamiltonian approaches.

## 5 LINE LISTS

DUO was used to solve the fully coupled Schrödinger equation for the four lowest bound electronic states of SiH using our refined curves. The details of the DUO methodology used for building accurate, empirical line lists for diatomic molecules has been extensively discussed elsewhere (Patrascu et al. 2014, 2015; Lodi et al. 2015; Tennyson et al. 2016b; Yurchenko et al. 2016). A grid-based sinc basis of 501 points spanning 1 to 4 Å was used, selecting the 40, 20, 40, and 10 lowest vibrational eigenfunctions of the  $X^2\Pi$ ,  $a^4\Sigma^-$ ,  $A^2\Delta$ ,  $B^2\Sigma^-$  states respectively.

The line list produced for  $^{28}\text{SiH}$  contains 1,724,841 transitions and 11,785 states covering frequencies up to  $31340 \text{ cm}^{-1}$ . The line lists for the isotopologues  $^{29}\text{SiH}$ ,  $^{30}\text{SiH}$  and  $^{28}\text{SiD}$  were generated using the same methodology by simply changing the nuclear masses to the corresponding values (see Table 5). For compactness and ease of use the line lists are separated into energy state and transitions files using the standard ExoMol format (Tennyson et al. 2016c). Tables 6 and 7 show extracts from the States and Transition files, respectively. The full line lists for all isotopologues considered can be downloaded from [www.exomol.com](http://www.exomol.com) and from the CDS database.

As part of the ExoMol line lists, we now provide lifetimes and Landé  $g$ -factors for the states involved (Tennyson et al. 2016a). The methodology used to compute them is detailed in Semenov et al. (2017). The lifetime of the  $A$  state ( $v = 0$ ,  $J \leq 11.5$ ) was measured in laser-induced fluorescence experiments by Bauer et al. (1984) to be  $534 \pm 23$  ns and by Schmitt et al. (1984) to be  $530 \pm 2$  ns, see also a review of other measurements by Bauer et al. (1984). Our value is 400 ns for the  $J' = 10.5$  ( $0-0$ ). Larsson (1987) in his CASSCF calculations showed that the  $X-A$  transition dipole moments depends strongly on the active space (see Table V of cited paper) and that the closest agreement with the experimental lifetime was not for the largest one. Among Larsson (1987)'s computed lifetimes the one closest to experiment is 484 ns ( $\mu_+ = 0.706$  D) using a 5-electrons in 9 orbitals ( $3\sigma, 2\pi, 1\delta$ ) active space. Using a similar 5-electrons in 10 orbitals active space comprising 5  $a_1$ , 2  $b_1$ , 2  $b_1$  and 1  $a_2$  orbitals we have obtained a similar value of the equilibrium dipole moment ( $\mu_+ = 0.706$  D). However, we could not converge our calculations of the DMC with this choice of the active space for all the geometries considered; we managed to obtain convergence for all values of  $r$  between 0.7 and 5 Å using the large 5-electrons in 15 orbitals active space described at the end of section 3 which, however, gave a slightly too high value of  $\mu_+$  (0.789 D). We therefore decided to re-scale the

**Table 3.** Example of Obs.–Calc. residuals, in  $\text{cm}^{-1}$ , for  $^{28}\text{SiH } v = 0$  levels illustrating the rotational accuracy of the  $X$  state of our refined model.

$J$	Parity	$\Omega$	Obs.	Calc.	Obs.-Calc.
0.5	–	–0.5	0.1000	0.0972	0.0028
1.5	+	0.5	21.0376	21.0336	0.0040
1.5	+	1.5	151.5592	151.5585	0.0007
1.5	–	–0.5	20.8457	20.8469	–0.0012
1.5	–	–1.5	151.5515	151.5510	0.0006
2.5	+	0.5	55.6671	55.6698	–0.0026
2.5	+	1.5	190.5415	190.5407	0.0009
2.5	–	–0.5	55.9368	55.9318	0.0050
2.5	–	–1.5	190.5710	190.5697	0.0013
3.5	+	0.5	104.8464	104.8407	0.0056
3.5	+	1.5	245.0493	245.0471	0.0021
3.5	–	–0.5	104.5183	104.5223	–0.0040
3.5	–	–1.5	244.9792	244.9780	0.0012
4.5	+	0.5	167.4554	167.4606	–0.0052
4.5	+	1.5	314.7410	314.7398	0.0013
4.5	–	–0.5	167.8197	167.8136	0.0061
4.5	–	–1.5	314.8734	314.8703	0.0031
5.5	+	0.5	244.9044	244.8982	0.0062
5.5	+	1.5	399.9092	399.9051	0.0042
5.5	–	–0.5	244.5274	244.5337	–0.0063
5.5	–	–1.5	399.6918	399.6907	0.0011
6.5	+	0.5	335.7692	335.7763	–0.0070
6.5	+	1.5	499.6914	499.6909	0.0005
6.5	–	–0.5	336.1354	336.1292	0.0062
6.5	–	–1.5	500.0167	500.0116	0.0051
7.5	+	0.5	441.5298	441.5240	0.0058
7.5	+	1.5	615.0542	615.0480	0.0061
7.5	–	–0.5	441.1975	441.2052	–0.0076
7.5	–	–1.5	614.5987	614.5994	–0.0006
8.5	+	0.5	560.8100	560.8179	–0.0079
8.5	+	1.5	744.2736	744.2760	–0.0024
8.5	–	–0.5	561.0863	561.0811	0.0052
8.5	–	–1.5	744.8800	744.8731	0.0069
9.5	+	0.5	694.7840	694.7799	0.0041
9.5	+	1.5	889.3533	889.3460	0.0074
9.5	–	–0.5	694.5847	694.5926	–0.0079
9.5	–	–1.5	888.5761	888.5810	–0.0049
10.5	+	0.5	842.4815	842.4890	–0.0075
10.5	+	1.5	1047.3665	1047.374	–0.0084
10.5	–	–0.5	842.5838	842.5813	0.0025
10.5	–	–1.5	1048.3332	1048.325	0.0076
11.5	+	0.5	1004.4299	1004.429	0.0004
11.5	–	–0.5	1004.4433	1004.450	–0.0070

(11,4,4,1) DMC by a factor  $\sqrt{400/530} \approx 0.869$ , thus bringing the lifetime of the  $J' = 10.5$  ( $0-0$ ) level to 530 ns. It should be noted that the lifetime of the  $v = 0$  state gradually increases to 800 ns at  $J = 32.5$ .

## 6 EXAMPLES OF SPECTRA

The temperature at which spectra are simulated has a strong effect on the intensities produced. Some examples of absorption spectra at different temperatures are presented in Fig. 6. The structure of the strongest electronic bands is shown in Fig. 7. The  $a^4\Sigma^- - X^2\Pi$  band is dipole forbidden but can ‘steal’ intensity by interacting with the  $X^2\Pi$  state. Considering the relative contrast of this band, it would be interesting to see attempts of detecting this bands experimentally.

### 6.1 Comparisons of spectra

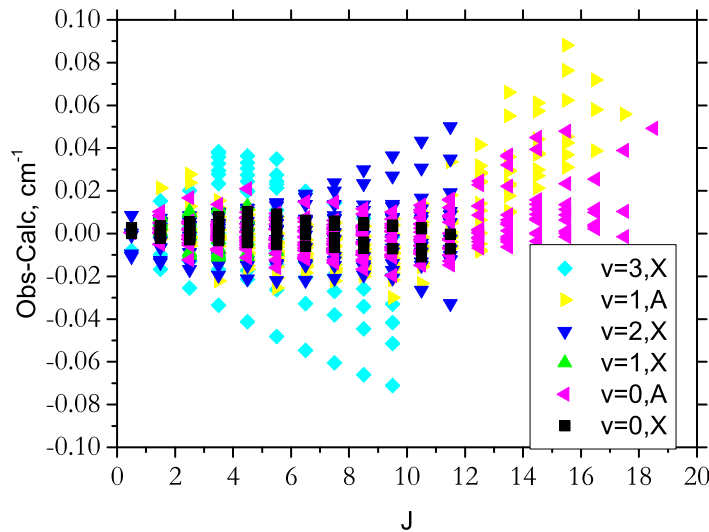
In order to test the quality of our theoretical line list, we present a number of comparisons with previous works. The CDMS catalogue contains a comparatively small number of transitions at low wavenumbers (Müller et al. 2005). For this reason, this work is only comparable in the ( $0-0$ ) band. The CDSM spectra include hyperfine splitting, which is ignored in our calculations. In order to provide a fair comparison of CDMS with our spectra, we have combined the CDMS hyperfine sub-structures into

**Table 4.** Example of Obs.–Calc. residuals, in  $\text{cm}^{-1}$ , illustrating the vibrational accuracy of our refined model. Energies for  $^{28}\text{SiH}$  are given relative to the  $v = 0, J = 0.5, +, \Omega = 0.5$  level.

$J$	Parity	State	$v$	$\Omega$	Obs.	Calc.	Obs.-Calc.
0.5	+	$X$	1	0.5	1970.3041	1970.3130	−0.0089
0.5	+	$X$	2	0.5	3869.6575	3869.6600	−0.0025
0.5	+	$X$	3	0.5	5698.7697	5698.7789	−0.0092
0.5	−	$X$	0	−0.5	0.0859	0.0972	−0.0113
0.5	−	$X$	1	−0.5	1970.4103	1970.4108	−0.0005
0.5	−	$X$	2	−0.5	3869.7405	3869.7585	−0.0180
0.5	−	$X$	3	−0.5	5698.8651	5698.8763	−0.0112
1.5	+	$X$	0	0.5	21.0376	21.0336	0.0040
1.5	+	$X$	0	1.5	151.5592	151.5585	0.0007
1.5	+	$X$	1	0.5	1990.7716	1990.7826	−0.0110
1.5	+	$X$	1	1.5	2122.1435	2122.1638	−0.0203
1.5	+	$X$	2	0.5	3889.5532	3889.5673	−0.0141
1.5	+	$X$	2	1.5	4021.7593	4021.7763	−0.0170
1.5	+	$X$	3	0.5	5718.0995	5718.1237	−0.0242
1.5	+	$A$	0	1.5	24268.0465	24268.0614	−0.0149
1.5	+	$A$	1	1.5	25928.2856	25928.2823	0.0033
1.5	−	$X$	0	−0.5	20.8283	20.8469	−0.0186
1.5	−	$X$	0	−1.5	151.5420	151.5510	−0.0090
1.5	−	$X$	1	−0.5	1990.5945	1990.5943	0.0002
1.5	−	$X$	1	−1.5	2122.1346	2122.1566	−0.0220
1.5	−	$X$	2	−0.5	3889.3696	3889.3775	−0.0079
1.5	−	$X$	2	−1.5	4021.7541	4021.7694	−0.0153
1.5	−	$X$	3	−0.5	5717.9357	5717.9355	0.0002
1.5	−	$A$	0	−1.5	24268.0560	24268.0614	−0.0054
1.5	−	$A$	1	−1.5	25928.2705	25928.2823	−0.0118

**Table 5.** Statistics for line lists for all four isotopologues of SiH.

	$^{28}\text{SiH}$	$^{29}\text{SiH}$	$^{30}\text{SiH}$	$^{28}\text{SiD}$
$J_{\text{max}}$	82.5	82.5	82.5	113.5
$\nu_{\text{max}} (\text{cm}^{-1})$	31337.3	31337.3	31337.3	31337.3
$E'_{\text{max}} (\text{cm}^{-1})$	31337.3	31337.3	31337.3	31337.3
$E''_{\text{max}} (\text{cm}^{-1})$	31337.3	31337.3	31337.3	31337.3
number of energies	11785	11796	11808	21230
number of lines	1724841	1726584	1728386	3520657

**Figure 5.** Visual representation of difference in calculated and experimentally measured frequencies as a function of  $J$  for low-lying vibrational states of  $^{28}\text{SiH}$  in its  $X^2\Pi$  and  $A^2\Delta$  electronic states.



**Table 6.** Extract from the states file of the  $^{28}\text{Si}^1\text{H}$  line list.

$n$	Energy ( $\text{cm}^{-1}$ )	$g_i$	$J$	$\tau$	$g$ -factor	Parity	$e/f$	State	$v$	$\Lambda$	$\Sigma$	$\Omega$
1	0.000000	4	0.5	inf	-0.000721	+	e	X2Pi	0	1	-0.5	0.5
2	1970.313482	4	0.5	8.4593E-03	-0.000723	+	e	X2Pi	1	1	-0.5	0.5
3	3869.660924	4	0.5	4.5247E-03	-0.000724	+	e	X2Pi	2	1	-0.5	0.5
4	5698.780278	4	0.5	3.2392E-03	-0.000725	+	e	X2Pi	3	1	-0.5	0.5
5	7458.470416	4	0.5	2.6176E-03	-0.000724	+	e	X2Pi	4	1	-0.5	0.5
6	9148.745041	4	0.5	2.2639E-03	-0.000723	+	e	X2Pi	5	1	-0.5	0.5
7	10768.764728	4	0.5	2.0464E-03	-0.000721	+	e	X2Pi	6	1	-0.5	0.5
8	12316.884393	4	0.5	1.9086E-03	-0.000717	+	e	X2Pi	7	1	-0.5	0.5
9	13749.386223	4	0.5	2.4180E+00	3.337141	+	e	a4Sigma	0	0	0.5	0.5
10	13790.645552	4	0.5	1.8223E-03	-0.000713	+	e	X2Pi	8	1	-0.5	0.5
11	15187.015658	4	0.5	1.7723E-03	-0.000709	+	e	X2Pi	9	1	-0.5	0.5
12	15859.208556	4	0.5	5.8285E-01	3.337143	+	e	a4Sigma	1	0	0.5	0.5
13	16502.475508	4	0.5	1.7500E-03	-0.000710	+	e	X2Pi	10	1	-0.5	0.5
14	17732.992112	4	0.5	1.7519E-03	-0.000707	+	e	X2Pi	11	1	-0.5	0.5
15	17783.585608	4	0.5	2.8270E-01	3.337142	+	e	a4Sigma	2	0	0.5	0.5
16	18874.096315	4	0.5	1.7780E-03	-0.000691	+	e	X2Pi	12	1	-0.5	0.5
17	19508.796071	4	0.5	1.6795E-01	3.337143	+	e	a4Sigma	3	0	0.5	0.5
18	19921.019747	4	0.5	1.8315E-03	-0.000671	+	e	X2Pi	13	1	-0.5	0.5
19	20868.688182	4	0.5	1.9204E-03	-0.000643	+	e	X2Pi	14	1	-0.5	0.5
20	21019.734154	4	0.5	1.1238E-01	3.337140	+	e	a4Sigma	4	0	0.5	0.5

 $n$ : State counting number. $\tilde{E}$ : State energy in  $\text{cm}^{-1}$ . $g_i$ : Total statistical weight, equal to  $g_{\text{ns}}(2J + 1)$ . $J$ : Total angular momentum. $\tau$ : Lifetime ( $\text{s}^{-1}$ ). $g$ -Landé factors. $+/-$ : Total parity. $e/f$ : Rotationless parity.

State: Electronic state.

 $v$ : State vibrational quantum number. $\Lambda$ : Projection of the electronic angular momentum. $\Sigma$ : Projection of the electronic spin. $\Omega$ : Projection of the total angular momentum,  $\Omega = \Lambda + \Sigma$ .**Table 7.** Extract from the transitions file of the  $^{28}\text{SiH}$  line list.

$f$	$i$	$A_{fi}$ ( $\text{s}^{-1}$ )	$\tilde{\nu}_{fi}$
1494	1882	6.5269E-07	21.092521
9460	9670	3.4859E-08	21.142047
6251	6561	1.1771E-09	21.143927
1582	1711	1.0066E-10	21.144601
575	706	2.0164E-11	21.145126
413	290	1.4640E-03	21.153921
6969	7067	7.8938E-10	21.161879
4731	5076	1.2289E-11	21.165181
2255	2642	5.3380E-11	21.170838

 $f$ : Upper state counting number; $i$ : Lower state counting number; $A_{fi}$ : Einstein-A coefficient in  $\text{s}^{-1}$ ; $\tilde{\nu}_{fi}$ : transition wavenumber in  $\text{cm}^{-1}$ .

single lines. As can be seen from Fig. 8, the line positions are very similar, but the intensities differ by about a factor of four. The latter is due to the difference in the dipole moments. The CDMS used the equilibrium *ab initio* dipole moment value 0.087 D by Meyer & Rosmus (1975), while our value is  $\mu_e$  is 0.097 D. With our state-of-the-art *ab initio* level of theory of MRCI/aug-cc-pwC5Z-DK we should provide a higher quality  $X-X$  dipole moment. More importantly, our calculations also fully incorporate the effect of zero-point vibrational motion into the dipole matrix element by using a proper averaging over the vibrational wavefunctions, which is important for this band due to the sign change of the DMC close to the equilibrium bond length, see Fig. 2. As the result, for the vibrationally averaged dipole moment  $\mu_0$  is 0.0474 D, i.e. significantly smaller (about half the size) than the equilibrium dipole moment. The corresponding intensities are therefore 4 times weaker than those predicted by CDMS. Such an overestimate would lead, for example, to fourfold under-estimates of the abundance of any observed SiH. We recommend that the CDMS data is updated.

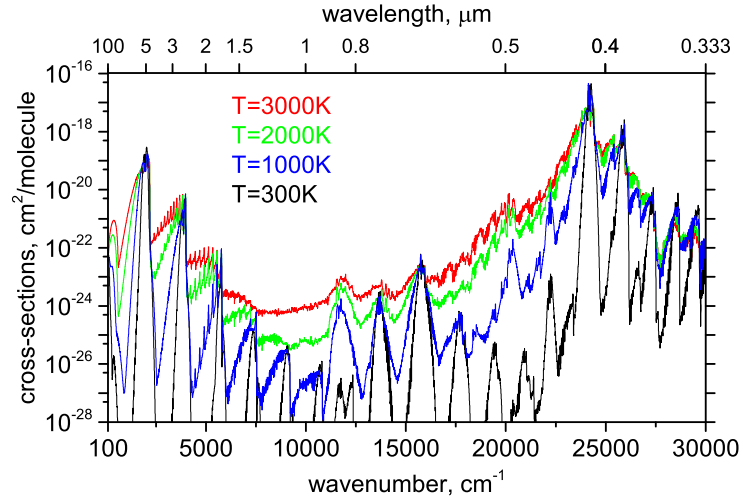


**Figure 6.** Comparison of the SiH absorption spectra at five different temperatures. The difference in intensity between 300 K and higher temperatures is most pronounced around  $20\,000\text{ cm}^{-1}$ .

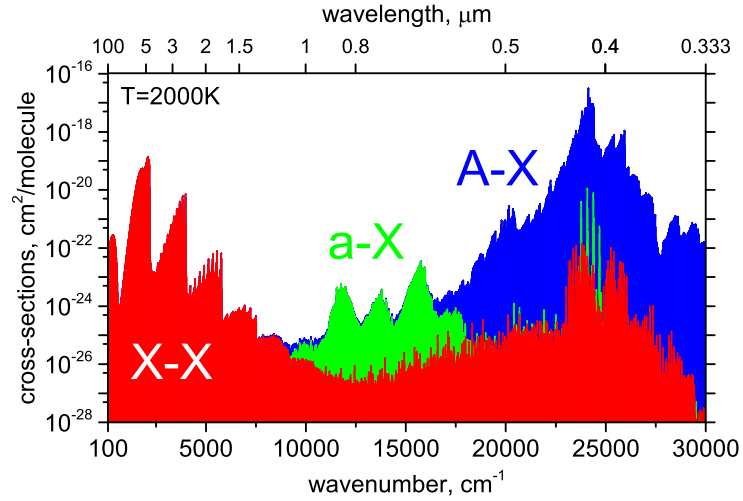


**Figure 7.**  $T = 2000\text{ K}$  absorption spectra of  $^{28}\text{SiH}$ : X-X,  $a$ -X, and A-X bands, where the  $a$ -X band is dipole forbidden.

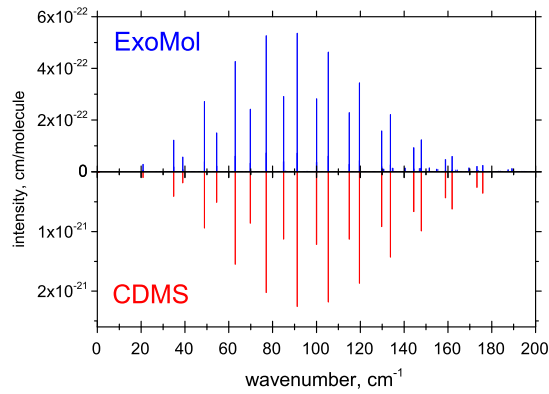


**Figure 8.** Comparison with available CDMS data for the  $(0-0)$  transitions of  $^{28}\text{SiH}$  at 298K. The difference in intensity is about 4.4 times due to the difference in the dipoles.

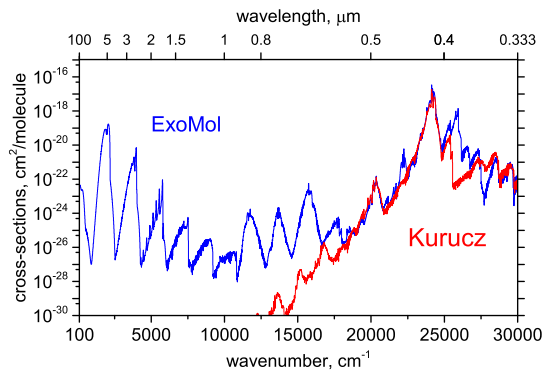


**Figure 9.** A comparison of absorption spectra produced from our line list with that of Kurucz (2011) at 1000K.

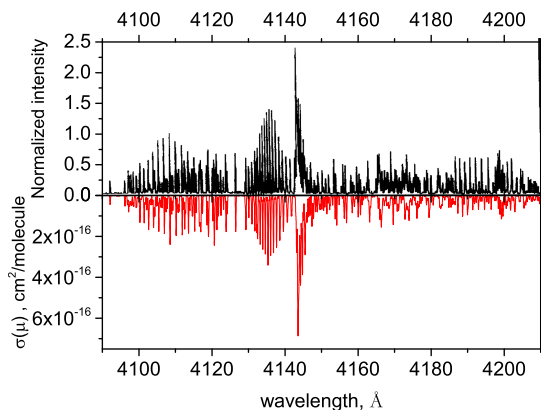


**Figure 10.** Upper display: Experimental emission spectrum of SiH from a 100 mTorr pure silane radio frequency discharge produced by Stamou et al. (1997) at 2000 K. Peak heights are normalised to the highest peak of the  $R_1$  branch,  $R_1(10.5)$ . Lower display: Theoretical emission spectrum of SiH at 2000 K. The peak intensities are similar to that from the experiment.

Figure 9 shows a comparison with a spectrum generated using the SiH line list by Kurucz (2011), where only the  $A-X$  transitions were included. These and other spectra presented in this work were computed using our new program EXOCROSS (Yurchenko et al. 2017). In the range where a comparison can be made (above 20 000  $\text{cm}^{-1}$ ), the main peak at 24 100  $\text{cm}^{-1}$  ( $0-0$ ) agrees quite well, while Kurucz’s ( $1-0$ ) and ( $0-1$ ) peaks on the right- and left-hand side from it are much weaker. The ( $2-0$ ) and ( $0-2$ ) bands agree well again, also for the absolute intensities. The disagreement could be due to our use of more modern experimental data, and to the use of higher level *ab initio* techniques, causing a discrepancy between the two results.

An additional measure of the accuracy of our line list is comparison to the experimental spectrum produced by Stamou et al. (1997), which is presented in Fig. 10. The basic shapes of the spectra are the same, with the peak intensity occurring close to 4140 Å which is taken to be the  $Q$  branch. Furthermore, additional peaks at 4130 Å and 4104 Å are replicated, as is the shape below 4100 Å. Differences in intensities arise at longer wavelengths (although the shape remains consistent), most likely because of the non-thermal effects not properly considered here (we assumed a Boltzmann distribution and used a Gaussian line profile of 0.5  $\text{cm}^{-1}$  HWHM).

## 6.2 Partition Function

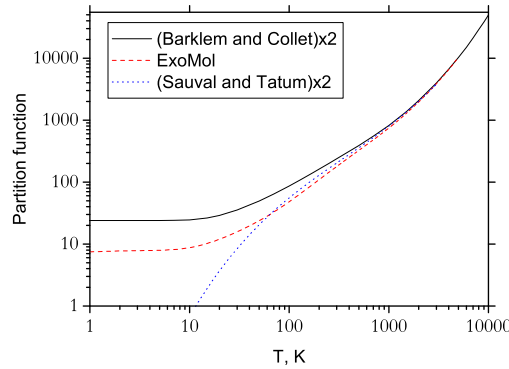
The partition function was calculated with DUO in steps of 1 K and was fitted to the following functional form (Vidler & Tennyson 2000) given by

$$\log_{10} Q(T) = \sum_{n=0}^8 a_n (\log_{10} T)^n. \quad (7)$$

The fitted expansion parameters for  $^{28}\text{SiH}$  are presented in Table 8. These parameters reproduce the temperature dependence of partition function of SiH with a relative root-mean-square error of 0.56 %; the fitting error increases to 1.8% at  $T = 5000$  K.

**Table 8.** Expansion coefficients for the partition function of  $^{28}\text{SiH}$  given by Eq. (7). Parameters for other isotopologues can be found in the supplementary material.

$a_i$	value
$a_0$	0.872519166079
$a_1$	0.331757300487
$a_2$	-1.370132158260
$a_3$	2.297149082100
$a_4$	-1.997501906630
$a_5$	1.134338070560
$a_6$	-0.384224515822
$a_7$	0.068401930630
$a_8$	-0.004881419966

**Figure 11.** A comparison between the partition function produced from our line list and the theoretical partition function described by Sauval & Tatum (1984). The latter values were multiplied by  $g_{\text{ns}} = 2$ .

This is still a very small error, and thus the fit can be said to reliably reproduce the partition function. The partition function and the expansion parameters for all four species are included into the supplementary materials.

Our partition function can be compared to that computed by Sauval & Tatum (1984) and by Barklem & Collet (2016). In order to directly compare with our calculated partition function, these partition functions need to be multiplied by the nuclear statistical weight  $g_{\text{ns}} = 2$  (Tennyson et al. 2016c). This is the so-called physics convention for the nuclear statistical weights, which ExoMol uses. Figure 11 shows this comparison. All three partition functions agree well at high temperature. The values given by Barklem & Collet (2016) at lower temperatures are too high. We believe that our function is sufficiently complete and more accurate at lower temperatures. At  $T = 75$  K our partition function 35.278 compares well to the CDMS's pure rotational value at  $T = 75$  K of 35.277; this agreement continues to very low temperature, where our partition function has the physically correct behaviour at  $T \rightarrow 0$  K:

$$Q(T) \approx 4(e^{-0 c_2/T} + e^{-0.097 c_2/T}) + \dots \quad (8)$$

where 4 is the total degeneracy, 0 and  $0.097 \text{ cm}^{-1}$  are the two lowest term values at  $J = 0.5$ , and  $c_2$  is the second radiation constant.

The nuclear statistical weights  $g_{\text{ns}}$  used to produce the partition functions for  $^{28}\text{SiD}$ ,  $^{29}\text{SiH}$ , and  $^{30}\text{SiH}$  (as well as their line lists) are 3, 4 and 2, respectively.

## 7 CONCLUSION

Accurate and complete line lists for  $^{28}\text{SiH}$  and three minor isotopologues  $^{29}\text{SiH}$ ,  $^{30}\text{SiH}$  and  $^{28}\text{SiD}$  have been produced, displaying good agreement with existing theoretical and experimental data. The accuracy of the rotational line positions is comparable to the one obtainable with effective rotational Hamiltonians. In order to reproduce the  $\Lambda$ -doubling splitting, an interaction via an electronic angular momentum coupling curve with the  $B^2\Sigma^-$  state was included using a very simple approximation to represent the PEC of the  $B$ -state.

The vibrationally averaged dipole moment  $\mu_0$  in the ground electronic state exhibit strong vibrational dependence and is about half in magnitude with respect to the equilibrium value. We suggest that the CDMS value of  $\mu_0$  should be updated.

The lifetimes computed for the  $A-X$  rotational transitions ( $J \leq 13.5$ ) using our best *ab initio* transition DMC ( $\approx 400$  ns) are off by about a factor 1.3 from the corresponding experimental values (530 ns). We use this experimental value to improve

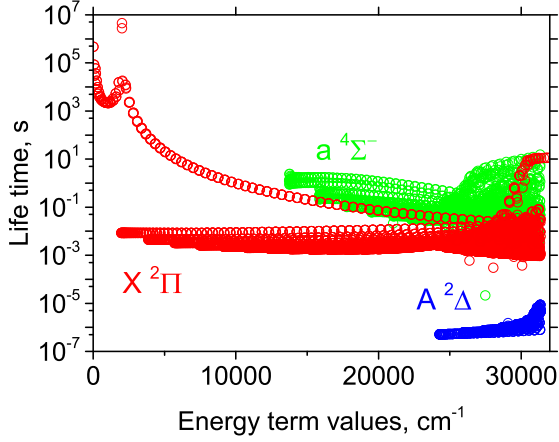


Figure 12. Lifetimes of the three lower electronic states of SiH.

the *ab initio* transition dipole moment curve by scaling it by a factor  $\sqrt{400/530} \approx 0.869$ , which leads to identical lifetimes (within 0.1 ns). A higher level of *ab initio* theory is therefore needed in order to be confident that the dipole moments used are accurate. It would also be beneficial to have more experimental data sensitive to the dipole moment, e.g. intensities or lifetimes.

## ACKNOWLEDGEMENTS

This work was supported by the UK Science and Technology Research Council (STFC) No. ST/M001334/1 and the COST action MOLIM No. CM1405. This work made extensive use of UCL's Legion high performance computing facility.

## REFERENCES

- Ajitha D., Pal S., 1999, *Chem. Phys. Lett.*, 309, 457  
Allard F., Hauschildt P. H., 1995, *ApJ*, 445, 433  
Allen W. D., Schaefer H. F., 1986, *Chem. Phys.*, 108, 243  
Babcock H. D., 1945, *ApJ*, 102, 154  
Baeck K. K., Lee Y. S., 1990, *J. Chem. Phys.*, 93, 5775  
Barklem P. S., Collet R., 2016, *A&A*, 588, A96  
Barton E. J., Yurchenko S. N., Tennyson J., 2013, *MNRAS*, 434, 1469  
Bauer W., Becker K. H., Düren R., Hubrich C., Meuser R., 1984, *Chem. Phys. Lett.*, 108, 560  
Berkowitz J., Greene J. P., Cho H., Ruscic B., 1987, *J. Chem. Phys.*, 86, 1235  
Betrencourt M., Boudjaader D., Chollet P., Guelachvili G., Morillonchapey M., 1986, *J. Chem. Phys.*, 84, 4121  
Bollmark P., Klynning L., Pagès P., 1971, *Phys. Scr.*, 3, 219  
Brown J. M., Merer A. J., 1979, *J. Mol. Spectrosc.*, 74, 488  
Brown J. M., Robinson D., 1984, *Mol. Phys.*, 51, 883  
Brown J. M., Watson J. K., 1977, *J. Mol. Spectrosc.*, 65, 65  
Brown J. M., Curl R. F., Evenson K. M., 1984, *J. Chem. Phys.*, 81, 2884  
Brown J. M., Curl R. F., Evenson K. M., 1985, *ApJ*, 292, 188  
Buenker R. J., 1986, *Intern. J. Quantum Chem.*, 29, 435  
Cade P. E., Huo W. M., 1967, *J. Chem. Phys.*, 47, 614  
Chang Y. W., Sun H., 2003, *Bull. Korean Chem. Soc.*, 24, 723  
Chang Y. W., Sun H., 2008, *J. Phys. Chem. B*, 112, 16135  
Cooper D. L., Richards W. G., 1981, *J. Chem. Phys.*, 74, 96  
Davies P. B., Isaacs N. A., Johnson S. A., Russell D. K., 1985, *J. Chem. Phys.*, 83, 2060  
Davis D. N., 1940, *PASP*, 52, 280  
Douglas A. E., 1957, *Can. J. Phys.*, 35, 71  
Drevillon B., Toulemonde M., 1985, *J. Appl. Phys.*, 58, 535  
Dunning T. H., 1989, *J. Chem. Phys.*, 90, 1007  
Freedman R. S., Irwin A. W., 1976, *A&A*, 53, 447  
Furtenbacher T., Császár A. G., 2012, *J. Quant. Spectrosc. Radiat. Transf.*, 113, 929  
Furtenbacher T., Császár A. G., Tennyson J., 2007, *J. Mol. Spectrosc.*, 245, 115  
Grant D. J., Dixon D. A., 2009, *J. Phys. Chem. A*, 113, 3656  
Grevesse N., Sauval A. J., 1970, *A&A*, 9, 232

- Grevesse N., Sauval A. J., 1971, *J. Quant. Spectrosc. Radiat. Transf.*, 11, 65
- Herbst E., Millar T. J., Wlodek S., Bohme D. K., 1989, *A&A*, 222, 205
- Herzberg G., Lagerqvist A., McKenzie B. J., 1969, *Can. J. Phys.*, 47, 1889
- Husain D., Norris P. E., 1979, *Faraday Discuss.*, 67, 273
- Huzinaga S., 1965, *J. Chem. Phys.*, 42, 1293
- Jackson C. V., 1930, *Proc. Roy. Soc. London A*, 126, 373
- Jasinski J. M., Becerra R., Walsh R., 1995, *Chem. Rev.*, 95, 1203
- Johnson R. D., Hudgens J. W., 1989, *J. Phys. Chem.*, 93, 6268
- Jun L., Jun L., Zhenfu H., Zhenyu D., 2010, *China Pet. Process. Petrochem. T.*, 12, 6
- Kalcher J., 1987, *Chem. Phys.*, 118, 273
- Kalemos A., Mavridis A., Metropoulos A., 2002, *J. Chem. Phys.*, 116, 6529
- Kampas F. J., Griffith R. W., 1981, *J. Appl. Phys.*, 52, 1285
- Kato H., 1993, *Bull. Chem. Soc. Japan*, 66, 3203
- Klynning L., Lindgren B., Sassenberg U., 1979, *Phys. Scr.*, 20, 617
- Kurucz R. L., 2011, *Can. J. Phys.*, 89, 417
- Lambert D. L., Mallia E. A., 1970, *MNRAS*, 148, 313
- Langhoff S. R., Davidson E. R., 1974, *Intern. J. Quantum Chem.*, 8, 61
- Larsson M., 1987, *J. Chem. Phys.*, 86, 5018
- Le Roy R. J., 2007, LEVEL 8.0 A Computer Program for Solving the Radial Schrödinger Equation for Bound and Quasibound Levels.  
University of Waterloo Chemical Physics Research Report CP-663, <http://leroy.uwaterloo.ca/programs/>
- Leroy G., Sana M., Wilante C., Tamsamani D. R., 1992, *J. Molec. Struct. (THEOCHEM)*, 91, 369
- Lodi L., Tennyson J., 2010, *J. Phys. B: At. Mol. Opt. Phys.*, 43, 133001
- Lodi L., Yurchenko S. N., Tennyson J., 2015, *Mol. Phys.*, 113, 1559
- Lovas F. J., 1974, *ApJ*, 193, 265
- Matsuda A., Nakagawa K., Tanaka K., Matsumura M., Yamasaki S., Okushi H., Iizima S., 1980, *J. Non-Cryst. Solids*, 35, 183
- Mauricio M. O., Roos B. O., Sadlej A. J., Dierksen G. H. F., 1988, *Chem. Phys.*, 119, 71
- McMillen D. F., Golden D. M., 1982, *Annu. Rev. Phys. Chem.*, 33, 493
- Medvedev E. S., Meshkov V. V., Stolyarov A. V., Ushakov V. G., Gordon I. E., 2016, *J. Mol. Spectrosc.*, 330, 36
- Merrill P. W., 1955, *PASP*, 67, 199
- Meyer W., Rosmus P., 1975, *J. Chem. Phys.*, 63, 2356
- Moore-Sitterly C., 1966, *Trans. Intern. Astron. Union B*, 12, 173
- Müller H. S. P., Schlöder F., Stutzki J., Winnewisser G., 2005, *J. Molec. Struct. (THEOCHEM)*, 742, 215
- Nemoto M., Suzuki A., Nakamura H., Shibuya K., Obi K., 1989, *Chem. Phys. Lett.*, 162, 467
- Owens A., Yurchenko S. N., Yachmenev A., Thiel W., Tennyson J., 2017, *MNRAS*, 471, 5025
- Park C., 1979, *J. Quant. Spectrosc. Radiat. Transf.*, 21, 373
- Park J. K., Sun H. S., 1992, *Chem. Phys. Lett.*, 195, 469
- Patrascu A. T., Hill C., Tennyson J., Yurchenko S. N., 2014, *J. Chem. Phys.*, 141, 144312
- Patrascu A. T., Tennyson J., Yurchenko S. N., 2015, *MNRAS*, 449, 3613
- Pearse R. W. B., 1933, in *Publications of the American Astronomical Society*. p. 12
- Perrin J., Delafosse E., 1980, *J. Phys.D: Appl. Phys.*, 13, 759
- Peterson K. A., Dunning T. H., 2002, *J. Chem. Phys.*, 117, 10548
- Pettersson L. G. M., Langhoff S. R., 1986, *Chem. Phys. Lett.*, 125, 429
- Prascher B. P., Lucente-Schultz R. M., Wilson A. K., 2009, *Chem. Phys.*, 359, 1
- Qui-Xia L., Tao G., Yun-Guang Z., 2008, *Chinese Phys. B*, 17, 2040
- Raghavachari K., Trucks G. W., Pople J. A., Head-Gordon M., 1989, *Chem. Phys. Lett.*, 157, 479
- Ram R. S., Engleman R., Bernath P. F., 1998, *J. Mol. Spectrosc.*, 190, 341
- Ramakrishna Rao T., Lakshman S., 1971, *Physica*, 56, 322
- Reiher M., 2006, *Theor. Chem. Acc.*, 116, 241
- Robertson R., Gallagher A., 1986, *J. Appl. Phys.*, 59, 3402
- Rochester G. D., 1936, *Z. Phys.*, 101, 769
- Rydbeck O. E. H., Elldér J., Irvine W. M., 1973, *Nature*, 246, 466
- Sauval A. J., 1969, *Sol. Phys.*, 10, 319
- Sauval A. J., Tatum J. B., 1984, *ApJS*, 56, 193
- Sax A. F., Kalcher J., 1991, *J. Phys. Chem.*, 95, 1768
- Schadee A., 1964, *B.A.N.*, 17, 311
- Schmitt J. P. M., Gressier P., Krishnan M., de Rosny G., Perrin J., 1984, *Chem. Phys.*, 84, 281
- Seebass W., Werner J., Urban W., Comben E. R., Brown J. M., 1987, *Mol. Phys.*, 62, 161
- Semenov M., Yurchenko S. N., Tennyson J., 2017, *J. Mol. Spectrosc.*, 330, 57
- Shi D.-H., Zhang J.-P., Sun J.-F., Zhu Z.-L., Yu B.-H., Liu Y.-F., 2008, *J. Molec. Struct. (THEOCHEM)*, 851, 30
- Shi D., Li P., Zhu Z., Sun J., 2013, *Spectra Chimica Acta A*, 115, 259
- Singh P. D., Vanlandingham F. G., 1978, *A&A*, 66, 87
- Smith W. H., 1969, *J. Chem. Phys.*, 51, 520
- Smith W., Liszt H., 1971, *J. Quant. Spectrosc. Radiat. Transf.*, 11, 45
- Song C., Gao T., Han H., Wan M., Yu Y., 2008, *J. Molec. Struct. (THEOCHEM)*, 870, 65
- Stamou S., Mataras D., Rapakoulas D., 1997, *Chem. Phys.*, 218, 57
- Stevens W. J., Krauss M., 1982, *J. Chem. Phys.*, 76, 3834
- Taniguchi M., Hirose M., Hamasaki T., Osaka Y., 1980, *Appl. Phys. Lett.*, 37, 787
- Tennyson J., 2014, *J. Mol. Spectrosc.*, 298, 1



- Tennyson J., Yurchenko S. N., 2012, [MNRAS](#), 425, 21
- Tennyson J., Yurchenko S. N., 2017, [Intern. J. Quantum Chem.](#), 117, 92
- Tennyson J., Hulme K., Naim O. K., Yurchenko S. N., 2016a, [J. Phys. B: At. Mol. Opt. Phys.](#), 49, 044002
- Tennyson J., Lodi L., McKemmish L. K., Yurchenko S. N., 2016b, [J. Phys. B: At. Mol. Opt. Phys.](#), 49, 102001
- Tennyson J., et al., 2016c, [J. Mol. Spectrosc.](#), 327, 73
- Turban G., Catherine Y., Grolleau B., 1980, [Thin Solid Films](#), 67, 309
- Turban G., Catherine Y., Grolleau B., 1981, [Thin Solid Films](#), 77, 287
- Turner J. L., Dalgarno A., 1977, [ApJ](#), 213, 386
- Verma R. D., 1965, [Can. J. Phys.](#), 43, 2136
- Vidler M., Tennyson J., 2000, [J. Chem. Phys.](#), 113, 9766
- Visscher C., Lodders K., Jr B. F., 2010, [ApJ](#), 716, 1060
- Washida N., Matsumi Y., Hayashi T., Ibuki T., Hiraya A., Shobatake K., 1985, [J. Chem. Phys.](#), 83, 2769
- Weinreb S., Barrett A. H., Meeks M. L., Henry J. C., 1963, [Nature](#), 200, 829
- Werner H. J., Knowles P. J., Lindh R., Manby F. R., Schütz M., 2010, MOLPRO, a package of ab initio programs
- Werner H.-J., Knowles P. J., Knizia G., Manby F. R., Schütz M., 2012, [WIREs Comput. Mol. Sci.](#), 2, 242
- Whiting E. E., Schadee A., Tatum J. B., Hougen J. T., Nicholls R. W., 1980, [J. Mol. Spectrosc.](#), 80, 249
- Wilson I. D. L., Richards W. G., 1975, [Nature](#), 258, 133
- Wilson R. W., Penzias A. A., Jefferts K. B., Kutner M., Thaddeus P., 1971, [ApJL](#), 167, L97
- Woon D. E., Dunning T. H., 1993, [J. Chem. Phys.](#), 98, 1358
- Yurchenko S. N., Lodi L., Tennyson J., Stolyarov A. V., 2016, [Comput. Phys. Commun.](#), 202, 262
- Yurchenko S. N., Al-Refaie A. F., Tennyson J., 2017, [Comput. Phys. Commun.](#), (submitted).
- de Almeida A. A., Singh P. D., 1978, [Astrophys. Space Sci.](#), 56, 415
- Šurkus A. A., Rakauskas R. J., Bolotin A. B., 1984, [Chem. Phys. Lett.](#), 105, 291

